WILEY-VCH

DOI: 10.1002/((please add manuscript number))
Article type: Communication

Electron Energy-Loss Spectroscopy of Spatial Nonlocality and Quantum Tunneling Effects in the Bright and Dark Plasmonic Modes of Gold Nanosphere Dimers

*Qiang Zhang, Xiangbin Cai, Xiang Yu, Susana Carregal-Romero, Wolfgang J. Parak, Ritesh Sachan, Yuan Cai, Ning Wang, Ye Zhu, Dang Yuan Lei**

Dr. Q. Zhang, Dr. Y. Zhu, Dr. D. Y. Lei
Department of Applied Physics
The Hong Kong Polytechnic University
Hung Hom, Hong Kong 999077, P. R. China
E-mail: dylei@polyu.edu.hk

Dr. X. Cai, Dr. Y. Cai, Prof. N. Wang
Department of Physics
The Hong Kong University of Science and Technology
Clear Water Bay, Hong Kong 999077, P. R. China

Dr. X. Yu, Dr. S. Carregal-Romero, Prof. W. J. Parak
Fachbereich Physik
Philipps Universität Marburg
Marburg, Germany

Dr. S. Carregal-Romero, Prof. W. J. Parak
CIC Biomagune
San Sebastian, Spain

Dr. X. Yu
Hubei Zhongpu Union Medical Science and Technology co., Ltd
Wuhan, P. R. China

Dr. R. Sachan
Materials Science and Technology Division
Oak Ridge National Laboratory
Oak Ridge, 37831, USA

Dr. D. Y. Lei
Shenzhen Research Institute
The Hong Kong Polytechnic University
Shenzhen 518055, P. R. China

Keywords: EELS, plasmonic dimers, spatial nonlocality, quantum tunneling, bright and dark modes

In this work, we present a theoretical and experimental electron energy-loss spectroscopy (EELS) study on gold nanosphere dimers with inter-particle distance d varying from ten nanometers to a few angstroms. Injecting an electron beam at the edge and the gap of the dimers excites their longitudinal bonding dipolar mode (BDM) and antibonding dipolar mode (ADM), respectively. Together with comprehensive EELS calculations within the frameworks of a local classical model, a nonlocal hydrodynamic model, and a quantum corrected model, we reveal that the spatial nonlocality and quantum tunneling phenomena have distinctively different effects on the plasmonic properties of BDM and ADM, such as resonant energy shift and intensity variation. Specifically, the spatial nonlocality effect blue-shifts the BDM energy and decreases its EELS intensity at $d < 3$ nm, while the quantum tunneling effect induces a much weaker charge transfer mode (CTM) at $d < 0.3$ nm. However, both effects have no impact on the ADM energy though they indeed affect its EELS intensity in dramatically different manners. The experimental EELS spectra at varied gap size measured with a scanning transmission electron microscopy (STEM) are qualitatively consistent with the numerical calculations. Our results may contribute to further understanding of quantum mechanical effects in different kinds of hybridized plasmon modes.

1. Introduction

It is well known that plasmonic nanoparticles made of noble metals such as gold and silver can interact strongly with the electromagnetic fields at optical frequencies, manifesting as the excitation of localized surface plasmon resonances (LSPRs).[1-4] When a LSPR occurs, the incident light can be strongly confined and enhanced in a deep sub-wavelength region. Such intriguing optical characteristics of LSPRs enable plasmonic nanostructures to have great applications in surface-enhanced Raman scattering (SERS),[5-7] ultrasensitive sensing,[8-10] plasmon-enhanced harmonic generation,[11-13] integrated optical circuits,[14, 15] light harvesting devices,[16-19] unidirectional scattering nanoantennas,[20] and plasmon enhanced strong light-

matter interaction,[21] etc. Among a variety of plasmonic structures, nanoparticle dimers, composed of two closely coupled nanoparticles, are of particular interest and importance in several aspects. Firstly, plasmonic dimers have a special significance in terms of understanding the electromagnetic coupling between different plasmon modes. For example, plasmon hybridization theory was developed from dimers and nowadays has become a canonical methodology to analyze the plasmon modes of other more sophisticated nanostructures.[22-28] Secondly, the light confinement and enhancement in the narrow gap region of dimers are usually much stronger as compared to individual nanoparticles.[29, 30] Therefore, a lot of photonic effects benefiting from strong local fields can be further strengthened by plasmonic dimers.[31-34] Thirdly, the strong Coulomb interactions between the plasmon-induced charges at the metal surfaces near the gap make plasmonic dimers an excellent candidate for exploring some quantum mechanical effects such as spatial nonlocality and quantum tunneling.[35-49] Regarding to these optical characteristics and applications of plasmonic dimers, one may find that the gap between the coupled particles plays a vital role. Many efforts have been devoted to study how the optical properties of plasmon modes of dimers depend on the gap size. For example, the scaling of the plasmon resonance wavelength of dimers with respect to the gap size has been exploited as one kind of nanometrology known as plasmon rulers.[50, 51] Nevertheless, when the gap is reduced down to the quantum regime, the spatial nonlocality and quantum tunneling will ruin this classical ruler equation.[52]

Based on the principle of plasmon hybridization, the LSPRs of a plasmonic dimer can be categorized to a bonding mode and an antibonding mode depending on their phase relation.[22] Generally speaking, the bonding and antibonding modes have different responses to an external field. For example, the longitudinal bonding dipolar mode (BDM) of a homodimer is considered as a “bright mode”, since it can be readily excited by a far-field source, e.g. a plane wave. On contrary, the longitudinal antibonding dipolar mode (ADM) is a “dark mode”, which is completely inert to the plane wave. Therefore, BDM has been more extensively

studied than ADM by many optical techniques based on far-field measuring tools, for example, dark-field scattering spectroscopy.[37, 53, 54] In this respect, inspecting optically dark modes demands sources such as local emitters and electron beams. Electron energy-loss spectroscopy (EELS) is such a powerful near-field measuring tool which has been frequently used to study the optically dark modes of plasmonic aggregates including nanoparticle dimers, trimers, tetramers and so on.[55-64] Moreover, due to the extremely high spatial resolution (<1 nm), EELS has also been demonstrated as a very effective approach to explore the nonlocal and quantum tunneling effects in plasmonic assemblies.[41, 45, 46, 65-67] However, most of these EELS studies are more concentrated on the bright plasmon modes, e.g. the longitudinal BDM in dimers,[41, 45, 46] while the nonlocal and quantum tunneling effect in dark plasmon modes are unexplored. Intuitively, the strong attractive Coulomb interaction of the induced charges renders quantum effects more conspicuous to be observed in the BDM by tracing the spectral evolution as gap size varies. Nevertheless, a comprehensive study on the nonlocal and quantum tunneling effects of dark plasmon modes is still meaningful to facilitate deeply understanding the quantum mechanical effects in strongly coupled plasmonic nanostructures.

Here we present an EELS study on gold nanosphere homodimers with varied gap size to explore the quantum effects on the longitudinal BDM (bright mode) and ADM (dark mode). The longitudinal BDM and ADM of the homodimers are excited respectively when the electron beam passes by the dimers at their edge and gap center. Firstly, we investigate the EELS spectra of the dimers by numerical calculations using the local classical model, the nonlocal hydrodynamic model[49, 68-70] and the quantum corrected model (QCM).[40,71] By analyzing the resonant energy and EELS intensity of the two modes as a function of gap size, we demonstrate that the nonlocal and quantum tunneling effects affect the plasmon properties of both BDM and ADM in dramatically different manners. For the BDM, the nonlocal effect comes into play when the gap size is smaller than 3 nm and results in apparent blue shift of the resonant energy and reduction of the EELS intensity. As the gap size is further decreased

into the quantum tunneling regime (0.2 ~ 0.3 nm), the BDM gradually disappears, while a charge transfer mode (CTM) is established by the tunneling current through the gap. For the ADM, however, neither the nonlocal effect nor the quantum tunneling has influences on its resonant energy, and only the EELS intensity is slightly different with that of the local classical model. Experimentally, we prepared the gold dimers whose gap size was precisely controlled by layer-by-layer assembled polymeric films as spacers between the adjacent particles. The EELS spectra of the samples and corresponding gap distances were measured with a scanning transmission electron microscope (STEM). Although the quantitative comparison between the experimental and numerical results are difficult due to the poor EELS signal-to-noise ratio and severe spectral broadening, the measured EELS spectra still show good agreement with the numerical results in several important aspects.

2. Result and Discussion

We begin the EELS study on the gold nanosphere dimers with numerical calculations using the commercial package COMSOL Multiphysics 4.3a (RF model). A two-step process is adopted to calculate the electron energy-loss probability Γ_{EELS} of the dimers. In the first step, the radiation fields of the electron beam in vacuum are computed by using a line current source. The electromagnetic field obtained from the first step is then used as the background field to calculate the EELS spectra of the dimers in the second step (see details in the Experimental Section).[66] **Figure 1a** sketches the simulation model in three-dimensional view (top panel) and two-dimensional cross-sectional view (bottom panel). For simplicity, in the simulations the dimers are composed of two equivalent gold nanospheres and assumed to be free standing in air. The diameter of the gold spheres is fixed as $D = 50$ nm and the face-to-face inter-particle distance, i.e. the size of the gap between them is denoted as d. To study the longitudinal modes only, the dimers are excited by an aloof electron beam passing perpendicularly (z-direction) with respect to the dimer axis at two different positions as

represented by the red and blue arrows in Figure 1a. One position is the center of the gap and the other one is at 2 nm away from the edge of the dimer. We choose an exemplary dimer with $d = 0.5$ nm to analyze the excited plasmon modes by the electron beam at the two positions. Here only the local classical response of the dimer is considered and the quantum effects will be discussed later. The calculated EELS spectra of the exemplary dimer are shown in **Figure 1b** with the red (blue) line corresponding to the electron beam at the edge (center) of the dimer. Clearly, there are three predominant peaks on the spectra with different resonant energies and line-widths. To discern these different hybridized plasmon modes, the surface charge distributions of the dimer at the corresponding resonant peaks are given in the insets of Figure 1b. It is seen that the mode with the lowest resonant energy $\omega_{res} \approx 2$ eV can be attributed to a longitudinal BDM characterized by an anti-symmetric dipolar charge distribution with respect to the vertical central line of the dimer. The charge distribution is not perfectly anti-symmetric because denser charges are induced at the particle edge which is closer to the electron beam. Such BDM has a constructive axial dipole moment and thus is an optical bright mode which can be also excited by an axially polarized plane wave. The second mode at $\omega_{res} \approx 2.4$ eV has a similar anti-symmetric charge distribution yet with one more neutral node, indicating that it is a higher order mode corresponding to a longitudinal bonding quadrupolar mode (BQM). Different from the edge excitation, when the electron beam is passing through the center of the gap only one plasmon mode is excited with the highest resonant energy $\omega_{res} \approx 2.48$ eV. Under such excitation, the overall system including the electron beam has a perfect mirror symmetry with respect to the vertical axis. As a result, the excited plasmon mode exhibits a symmetric charge distribution as shown in the inset and can be attributed to a longitudinal ADM. Apparently, this ADM has a zero net dipole moment and thus cannot be excited by a plane wave, that is, an optically dark mode. We see from Figure 1b that the bonding and antibonding modes can be independently excited by the electron

beam either at the edge or center of the dimer. Together with the sub-nanometer spatial resolution of STEM, the EELS measurement provides us an excellent method to comparatively investigate the quantum mechanical effects in those hybridized plasmon modes of the dimer at the truly nanoscale level.

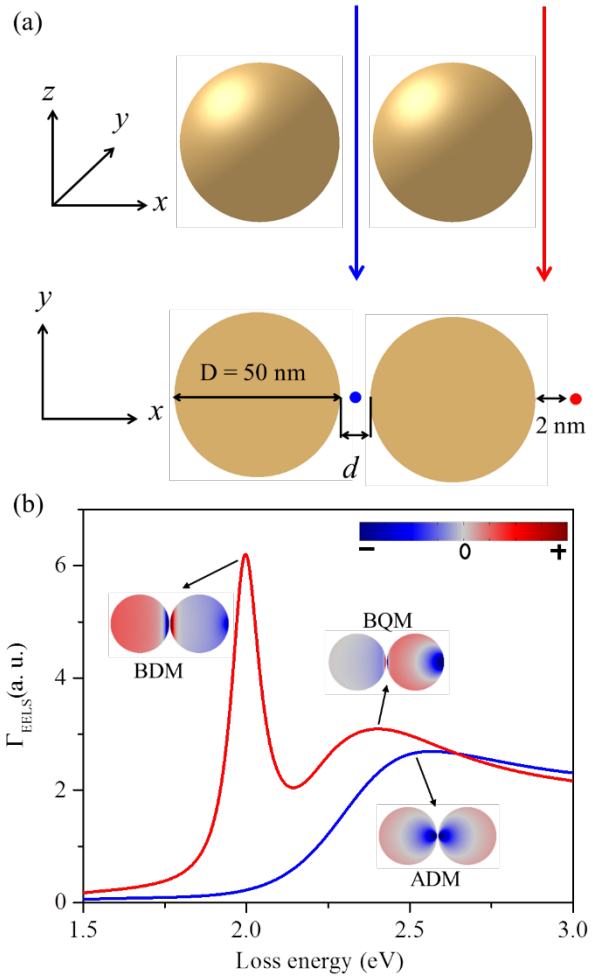

Figure 1. a) Schematic of a gold nanosphere homodimer and our EELS calculation model. The color arrows denote the electron beams incident at two different positions. b) Calculated EELS spectra for a gold nanosphere dimer with $d = 0.5$ nm under the edge (red) and center excitation (blue).

We then extend our EELS calculations by incorporating the nonlocal and quantum effects through combining with a hydrodynamic model and a QCM, respectively. Both effects can be implemented in a classical electromagnetic simulation (see details in the Experimental Section).[40, 66, 71] For the comparison purpose, we firstly consider the edge excitation and show the corresponding EELS spectra for the dimers with gap size varied from 0.2 nm to 10

nm in **Figure 2a**. For each dimer, we calculate its EELS spectrum by the local classical model (black-solid lines), the nonlocal hydrodynamic model (red-dashed lines), and the QCM (blue-dash-dotted lines). It is found that at $d > 0.5$ nm the EELS spectra obtained by the QCM are exactly the same as the classical results (so the QCM spectra for the dimers with $d > 1$ nm are not shown here). Figure 2a shows that the spectra of classical, nonlocal, and QCM evolve differently as the two particles get close to each other. Specifically, the classical EELS spectra show a single resonance peak when the particles are largely separated ($d > 1$ nm). This EELS peak corresponds to the longitudinal BDM as we discussed in Figure 1b, except for a much broader line-width due to the larger loss of gold in the long wavelength regime. The resonant energy of this longitudinal BDM red-shifts as the gap size decreases, consistent with the principle of the plasmon hybridization theory.[22] As the particles move away from each other, they become decoupled and finally converge to the case of an individual gold sphere whose dipolar resonance is at 2.48 eV. For the higher order bonding mode BQM, it appears only at very small gap distance ($d < 1$ nm) and its resonant energy is less sensitive to the gap size. In the classical framework, the EELS spectra in Figure 1a will become divergent when the particles further approach to the limiting case i.e. $d \to 0$, due to the excitation of too many higher order modes. Such divergence is essentially caused by an abrupt boundary in classical theory, assuming that the induced surface charges exist in a surface layer with ideally zero thickness.[70, 71]

It has been demonstrated that the spatial nonlocality in gold nanosphere dimers becomes prominent when the gap size is smaller than ~3 nm.[47, 48] One of the most important effects of spatial nonlocality is the blue-shift of the BDM energy compared to the local classical prediction. This is verified in Figure 2a that the BDM energies of the nonlocal spectra (red-dashed lines) are clearly higher than those of the local spectra, especially in the regime of $d < 1$ nm. The spatial nonlocality induces volume charge density inside the metal in a layer whose thickness is on the order of the Fermi wavelength (about 0.5 nm for gold).[66, 72]

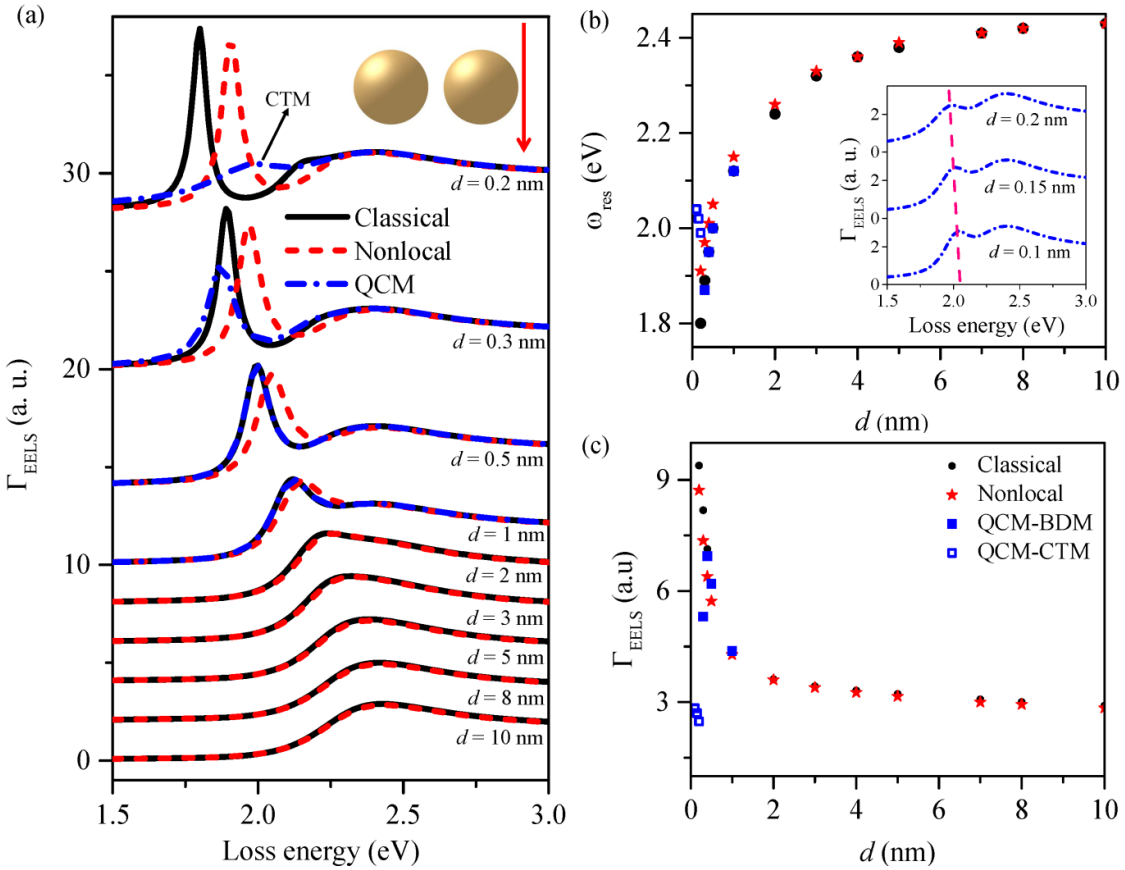

Figure 2. The EELS properties of the homodimers under the edge excitation. a) Simulated EELS spectra of the homodimers with gap size d varied from 0.2 nm to 10 nm obtained by the local classical model (black-solid lines), the nonlocal hydrodynamic model (red-dashed lines), and the QCM (blue dash-dotted lines). b) The resonant energy of the BDM (solid symbols) and the CTM (hollow symbols) as a function of the gap size d extracted from (a). The inset shows the QCM spectra of the dimers with gap size below 0.2 nm and the pink line marks the trace of the resonant energy of the higher order CTM. c) The EELS peak intensity of the BDM and the CTM as a function of the gap size d extracted from (a).

Thus the centroid of the charge density near the gap has a displacement inward to the metal surface, leading to a larger effective gap distance. In this perspective, the blue-shift in resonance energy of the BDM by the nonlocal effect can be readily understood as a result of increased effective gap size.[71, 73] In addition to the resonant energy, it is also worth to note that the EELS peak intensity of the BDM is also reduced by the nonlocal effect. The EELS intensity reduction is related to the nonlocality induced field quenching effect, because it is directly determined by the z-component of the induced near-field (see details in the Experimental Section). As the gap size further decreases to the atomic scale, the electron clouds of the surface charges near the gap overlap and the quantum tunneling emerges.

Despite of the fact that a more rigorous description of the quantum tunneling effect requires full quantum mechanical treatment such as using the time-dependent density function theory, the QCM developed by Esteban et al. provides a semi-classical and easy-to-implement approach that can generally capture the key features of electron tunneling.[40] The EELS spectra of the QCM and classical calculations shown in Figure 2a have no difference until the gap size is decreased down to $d = 0.3$ nm where the BDM resonant peak has an obvious intensity reduction, indicating its gradual disappearance in the spectrum. As the gap size is further decreased to $d = 0.2$ nm, the BDM completely disappears because the vacuum gap is finally short-circuited by the tunneling current. Meanwhile, a new mode shows up at the energy slightly lower than the BQM, which is attributed to a higher-order CTM. Our QCM calculations are consistent with previous experimental surface-enhanced Raman scattering spectroscopy and semi-classical theoretical studies that have demonstrated the quantum tunneling effect of a gold nanosphere dimer occurs in a gap size range of 0.3 nm~0.5 nm.[36, 40] On the other hand, we notice that the spatial nonlocality and quantum tunneling effects have negligible impact on the resonance energy and intensity of the BQM.

The EELS energy and peak intensity of the BDM extracted from Figure 2a as a function the gap size are shown in **Figure 2**b and **2**c (blue-solid-squares), respectively. We also calculate the EELS spectra of three dimers with gap size below 0.2 nm by the QCM (see the inset in Figure 2b) and trace the resonant energies of the higher-order CTM by the wine-red dashed line. To distinguish the CTM from the BDM, the EELS energy and peak intensity of the CTMs are given in Figure 2b and 2c with the blue-hollow-squares, respectively. Clearly, the BDM and CTM have quite different responses to the gap size variation. In particular, the CTM blue-shifts as the gap size decreases and has much weaker EELS intensity than the BDM. Although the nonlocal and tunneling effects are separately studied in Figure 2, these two effects in fact work together in the limiting case $d \to 0$. Numerically we are able to combine the hydrodynamic model and the QCM to consider them simultaneously, such

calculation has been done by Esteban et al. and it turns out that the tunneling effect is dominant when d is smaller than 0.3 nm.[71] Specially, the vanishing of the BDM and appearance of the CTM is caused by the quantum tunneling effect. Numerically, we implement the Hydrodynamic model and the QCM separately to distinguish the influence of the nonlocal effect and the quantum tunneling effect. Results in **Figure 2** indicate the plasmon properties of the BDM are strongly affected by both, the spatial nonlocality and quantum tunneling effect.

We next turn to investigate the EELS responses of the homodimers under the center excitation in **Figure 3**. Similarly, the EELS spectra of the dimers with gap size $d > 1$ nm calculated by the QCM are identical to the classical spectra and thus are not shown. All the EELS spectra in **Figure 3a** present a single peak which can be attributed to the ADM (see Figure 1b). More importantly, compared to the case of edge excitation (Figure 2), the EELS spectra calculated by different models in Figure 3a have little difference. This can be more specifically learned from the EELS energy and intensity of the ADM as a function of gap size as shown in **Figure 3b** and **3c**. In accordance with the plasmon hybridization theory, the resonant energy of the ADM blue-shifts very slowly as the gap size reduces as seen in Figure 3b and the ADM energies obtained by different calculation models are nearly the same. In addition, the nonlocal results give rise to weaker EELS intensity than the classical ones as seen in Figure 3c. However, the intensity reduction of the ADM by the nonlocal effect is still smaller than that of the BDM (note that the scale of y-axis of Figure 3c is smaller than that of Figure 2c). Therefore, we conclude that the spatial nonlocality also has influence on the plasmon properties of the ADM, but the effect is much weaker than the BDM. In particular, the resonance energy of the ADM is not shifted by the nonlocal effect [see results shown in Figure 3(b)]. This can be understood by the fact that the resonance energy of the BDM is essentially not so sensitive to the gap size [Figure 3(b)] when compared to the BDM [Figure 2(b)]. In point of this, the increased effective gap size of the dimer by the nonlocal effect must

have little effect on the resonance energy of the ADM. Before discussing the QCM results of the ADM, we should realize that the quantum tunneling requires a potential difference across the gap. For the BDM, such potential difference is provided by the opposite plasmon-induced surface charges beside the gap. But the plasmon-induced surface charges of the ADM are of the same sign beside the gap (see the inset of Figure 1b), leading to equal potential of the coupled particles. In view of this, we expect that real quantum electron tunneling is not allowed for the ADM. Nevertheless, numerically the QCM can still be applied to obtain the EELS properties of the ADM in Figure 3. Firstly, the ADM energy obtained by the QCM in Figure 3b is always equivalent to that of the classical calculation, no matter how small the gap size is. This is consistent with the expectation that the quantum tunneling effect cannot occur for the ADM. However, the QCM EELS intensity shown in Figure 3c is larger than the classical calculations when the gap size is smaller than 0.3 nm. Such abnormal enhancement in EELS intensity is actually due to the bulk loss of the fictional medium in the gap region used in the QCM (see details in the Experimental Section). Inspecting the permittivity $\varepsilon_{\text{gap}}(\omega)$ of the fictional medium in the gap, we can see that when the gap size is much larger than the atomic scale, the fictional medium behaves like the vacuum because of $\varepsilon_{\text{gap}}(\omega) \approx \varepsilon_0 = 1$, where ε_0 is the relative permittivity of the vacuum. This explains why the QCM results are the same as the classical results for the dimers with large gaps. When the gap size goes to zero the fictional medium essentially behaves like the metal, i.e. $\varepsilon_{\text{gap}}(\omega) \approx \varepsilon_{\text{m}}(\omega)$, where $\varepsilon_{\text{m}}(\omega)$ is the permittivity of the metal. Thus, for the center excitation the electron beam actually penetrates a gold-like fictional medium when the gap size is smaller than 0.3 nm and will suffer additional bulk losses. However, we should keep in mind that such intensity enhancement is totally caused by the numerical calculation rather than the real physical effect. Despite of such extra bulk loss of the fictional medium, the QCM predicts reasonable spectral features that imply the quantum tunneling is forbidden in the ADM.

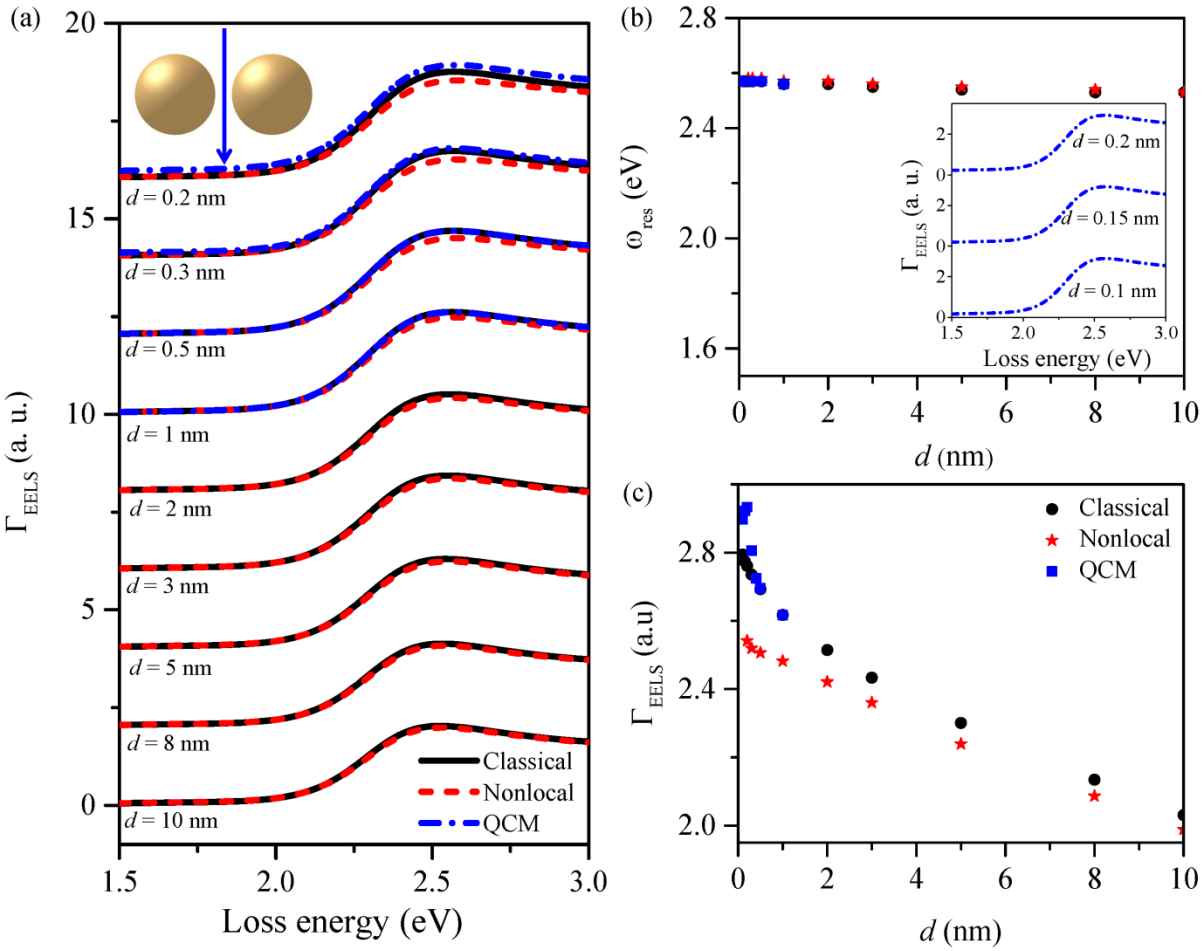

Figure. 3 The EELS properties of the homodimers under the center excitation. a) EELS spectra of the homodimers with gap size d varied from 0.2 nm to 10 nm calculated by the local classical (black solid lines) model, the nonlocal hydrodynamic model (red dashed lines), and the QCM (blue dash-dotted lines). b) The resonant energy of the ADM extracted from (a) as a function of the gap size d. The inset shows the QCM spectra of the dimers with gap sizes of 0.2, 0.15 and 0.1 nm. c) The EELS peak intensity of the ADM extracted from (a) as a function of the gap size d.

Figure 2 and 3 reveal that both, the EELS energy and intensity of the BDM is more likely to be affected by the nonlocal and quantum tunneling effects than the ADM. For the ADM, only its EELS intensity is slightly reduced by the nonlocality while the quantum tunneling cannot occur. To further understand such difference, we plot the near-field distribution profiles of the BDM, CTM, and ADM in the dimer with gap size of $d = 0.2$ nm in **Figure 4**. **Figure 4a** shows the near-field amplitude enhancement characterized by $\left|E_x^{\text{ind}}/E_x^{\text{b}}\right|$ of the BDM (classical and nonlocal) and the CTM (QCM) along the axis of the dimer, where E_x^{ind} is the x-component of the plasmon-induced field and E_x^{b} is the x-component of the background

field produced by the electron beam. Since the field "hot spot" of the BDM mainly resides in the gap, here we only show the region very close to the gap (-3 nm to 3 nm). As expected, the near-field enhancement of the BDM obtained by the classical (black solid line), nonlocal (red dashed line) model, and QCM (blue dash-dotted line) calculations exhibits great difference. Compared to the classical calculation that shows a maximum field enhancement of 5500 in the gap region at the BDM resonance energy, the nonlocal field enhancement is reduced to a maximum of 3000. Such decreasing of field strength caused by the spatial nonlocality can also be considered as a result of the induced larger effective gap size. Although the nonlocal effect can avoid the infinitely large field intensity in the gap region in the limiting case ($d \to 0$), the field enhancement is still very large due to a large number of bound ions and electrons accumulated on the metal surfaces near the gap. Considering the quantum tunneling effect, Figure 2 shows that the BDM is totally quenched at a gap size of 0.2 nm and a higher order CTM appears, so the near-field enhancement calculated by the QCM in Figure 4a is for this higher-order CTM instead of the BDM. It is seen that the field enhancement at the CTM resonance energy is one order smaller than the classical and nonlocal results. The contrast of the field enhancement calculated by the classical, nonlocal and QCM is more clearly seen in **Figure 4b** which shows the corresponding 2D field distributions. In addition, the nonlocal field enhancement curve in Figure 4a shows a different profile across the gap ($x = \pm 0.1$ nm) compared to the classical and QCM ones. This is because of an additional boundary condition (ABC) $\hat{\mathbf{n}} \cdot \mathbf{J} = 0$ used in the hydrodynamic model (see details in the Experimental Section), where $\mathbf{n}$ is the normal vector of the particle surface and $\mathbf{J}$ is the induced current density. In terms of the normal component of the electric field, such ABC implies $\varepsilon_{\text{core}}(\omega)\mathbf{E}_{\text{m}} \cdot \mathbf{n} = \varepsilon_0 \mathbf{E}_{\text{b}} \cdot \mathbf{n}$, where $\mathbf{E}_{\text{m}}$ ($\mathbf{E}_{\text{b}}$) is the electric field in the metal (background media), $\varepsilon_{\text{core}}(\omega)$ is the local permittivity of gold responsible for the bound ions and electrons. For pure electron plasma since $\varepsilon_{\text{core}}(\omega) = \varepsilon_0 = 1$ such ABC leads to the continuity of the normal electric field across the

interface between metal and the dielectric, indicating zero surface charge density on the boundaries.[49] However, for actual noble metals such as gold, $\varepsilon_{\text{core}}(\omega) \neq 1$ and the bound charges still accumulate on the metal surface, yielding the discontinuity of the normal electric field across the metal boundaries. So, physically speaking the discontinuity of the normal electric field across the gap as predicted by the Hydrodynamic model is reasonable. In sharp contrast, the near-field properties of the ADM shown in **Figure 4c** and **4d** show that the "hot spots" at the ADM resonance energy locate at the outer surfaces of the dimer rather than in the gap and the maximum field enhancement is much smaller than that of the BDM. This can be understood by the mirror-symmetric surface charge distribution at the ADM energy: the same sign of the surface charges near the gap leads to zero electric field at the center of the gap. Therefore the field quenching caused by the nonlocal effect is also weak for the ADM, leading to slightly reduced nonlocal EELS intensity as shown in Figure 3(b). Moreover, the near-field properties of different calculation models are nearly the same except that the nonlocal field profile at the outer boundaries is also slightly modulated by the ABC. These near-field characteristics in Figure 4 further demonstrate the significantly different influences of nonlocal and quantum tunneling on the hybridized BDM and the ADM.

Experimentally, we prepared the gold nanosphere dimers with controlled gap distance with electrostatically-driven linkage via polymeric spacers. Individual gold nanospheres were covered by alternating layers of cationic and anionic charged polymers, and then mixed together to form dimers by electrostatic adsorption. In this manner, the interparticle size, i.e. the gap size can be precisely controlled by the total number of the polymer layers (i.e. the more alternating layers are used, the thicker the polymer spacer becomes).[74] EELS spectra of the dimers with different gaps were then measured by STEM along with respective high-angle annular dark-field (HAADF) images. **Figure 5** shows the HAADF images and the corresponding image intensity profiles of five measured dimers with varied gap size. The imaging intensity profiles are collected from the HAADF images in regions enclosed by the

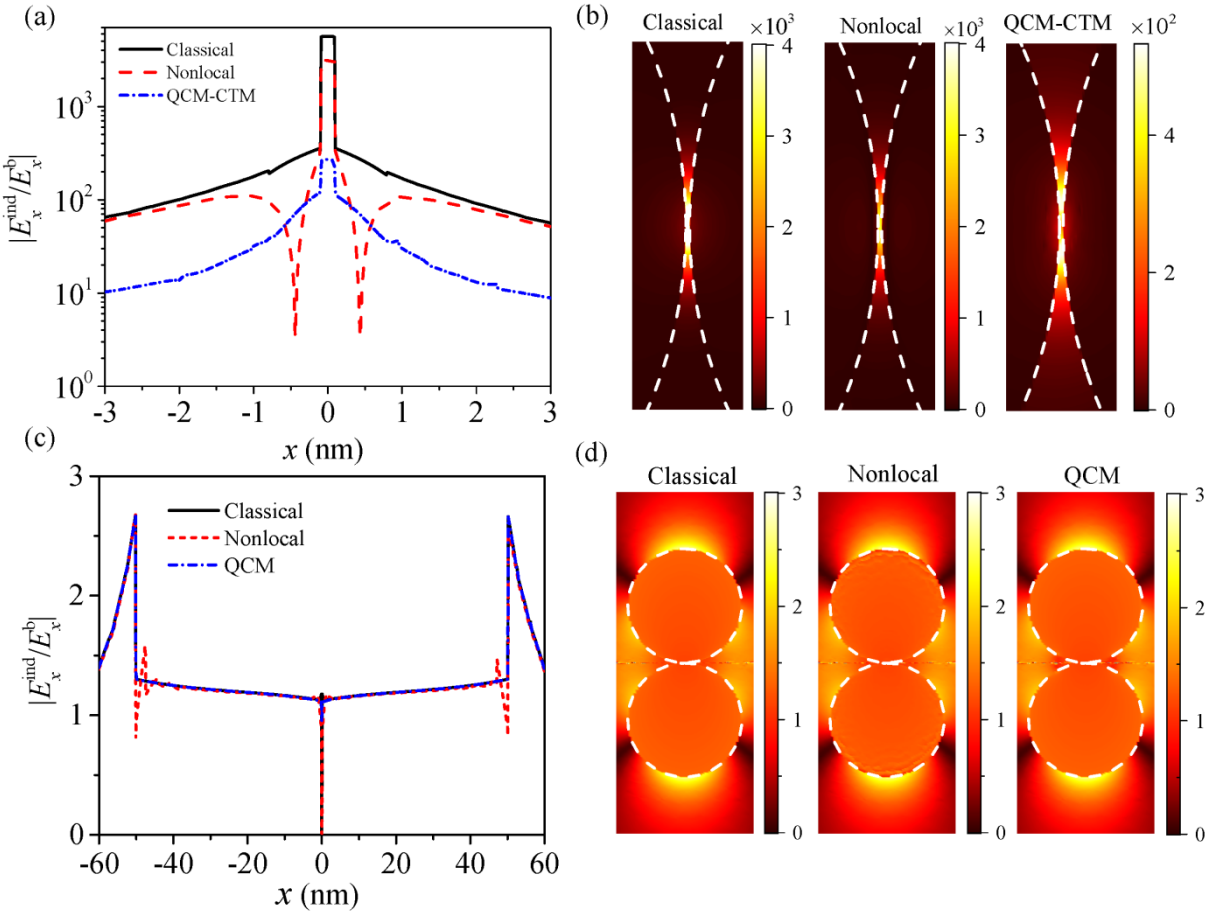

Figure 4. Near-field properties of the dimer with $d = 0.2$ nm characterized by $\left|E_x^{\text{ind}}/E_x^{\text{b}}\right|$ which is the *x*-component of the induced electric field E_x^{ind} normalized to the background field E_x^{b}. a) Calculated $\left|E_x^{\text{ind}}/E_x^{\text{b}}\right|$ profile along the horizontal central axis of the dimer under the edge excitation. The classical and nonlocal profiles correspond to the BDM while the QCM profile is for the higher-order CTM. Their 2D field maps are given in b). Correspondingly, c) and d) are the results for the ADM under the center excitation.

green vertical narrow rectangles of 5 nm width. The gap sizes can be determined by the distances between the two red horizontal lines aligned to the edges of the cliffs of the intensity profiles near the gap. The measured gap size of each dimer is labeled in Figure 5, which are $d = 0.5 \pm 0.1$ nm, $d = 0.8 \pm 0.1$ nm, $d = 1.4 \pm 0.1$ nm, $d = 2.8 \pm 0.2$ nm, and $d = 6.3 \pm 0.2$ nm. Note that while the gap size is well defined, the individual Au particles are not perfectly spherical and also have a certain size distribution.

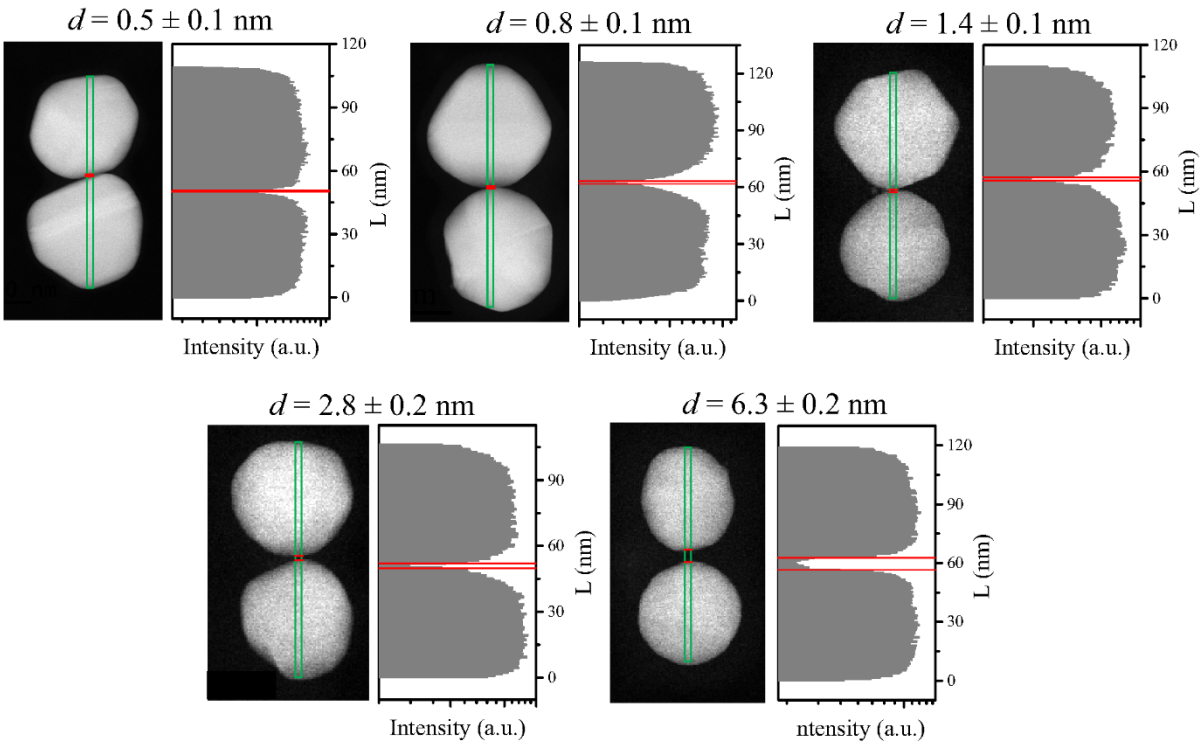

Figure 5. Experimentally measured HAADF images of five gold nanosphere dimers (left panels) and the corresponding profiles of imaging intensity (right panels) used for the gap size estimation. The intensity profiles are collected in the regions enclosed by the green rectangles with width of 5 nm in the images. The gap sizes are estimated by the distances between the red horizontal lines aligned to the edges of the deepest cliffs of the intensity profiles near the gap.

Figures 6a and **6b** show the measured EELS spectra of the dimers under the edge and center excitations, respectively. Theoretically, we have shown in Figure 2 that the BDM red shifts and its Q factor increases as the gap size decreases until it is quenched by the quantum tunneling effect when the gap size is smaller than 0.3 nm. Nevertheless, the experimentally collected EELS signals of the BDMs of the dimers with small gap size ($d < 3$ nm) are not observed in Figure 6a. This absence of EELS signals of the BDM for the dimers with gap size $d < 3$ may be caused by several possible reasons. The most likely reason is that in our experiments the dimers were supported by a carbon substrate which contributes to significant noisy background EELS signals at lower energies (below 2 eV). The second reason is because the BDM resonant energy of the dimers with small gaps is close to the zero loss peak of the electron beam. Thirdly, the quantum tunneling effect indeed occurs when the gap size is at the sub-nanometer level. Notwithstanding, the numerical results in Figure 2 predict the critical

gap size allowing the electron tunneling effect is smaller than 0.3 nm, but in experiments it is unlikely to determine this exact critical gap size. Note that the gap size measured in Figure 5 is an average estimation in a 5 nm width region that should be larger than the actual minimum face-to-face inter-particle distance. In fact, we also cannot ensure that the two particles in each dimer with a sub-nanometer gap have no touching point. More accurate morphological determination of the gap regions requires some advanced three-dimensional electron tomography imaging techniques [75-77]. In addition, in the experiment the gold nanospheres were coated with polymeric layers, indicating possible formation of polymer-filled gaps in the dimers (rather than vacuum gaps in theory). Several recent studies have revealed that the quantum tunneling effect can happen in a larger distance in a molecular-linked gap than the theoretical prediction for a vacuum gap (0.3 ~ 0.5 nm).[36, 37, 39, 46] Thus, possible presence of charged polymer molecules in the gap region of the fabricated dimers could promote the electron tunneling process at larger gap distances. However, the noisy background signals from the substrate make it difficult to explicitly observe the quantum effects in dimers with small gaps, for example the numerically predicted CTM can't be identified from the experimental spectra. More convincing experimental EELS signals at low energy range can be obtained with the state-of-the-art STEM instruments that yield <0.01 eV energy resolution, thus much narrower zero loss peak, and with the large-band-gap substrate such as silicon nitride or silicon dioxide.

Despite of the unreliable EELS signals at energy below 2 eV, the EELS spectra for $d = 0.5$ nm, $d = 0.8$ nm and $d = 1.4$ nm in Figure 6a show a set of EELS peaks locating at the same energy around 2.3 eV. According to the numerical results in Figure 2, we speculate that this set of EELS peaks corresponds to a higher-order bonding mode, most likely to the BQM which can be excited only in the dimers with relatively small gap sizes. The observation of the BQM in the experimental EELS spectra indicates that the influence of the background signals can be ignored at high energy range (beyond 2 eV). As a result, the BDM resonances of

dimers with large gap sizes (2.8 nm and 6.3 nm) can still be recognized in the experimental EELS spectra. Compared to the results of edge excitation shown in Figure 6a, the measured EELS spectra of the center excitation in Figure 6b have only one set of high-energy peaks which unambiguously come from the ADMs. The measured EELS peaks of the ADMs are present for all the dimers even those with sub-nanometer gaps. This is consistent with the numerical prediction in Figure 3 and further confirms that the quantum tunneling effect is forbidden for the ADM. To analyze the measured resonant energies of the hybridized modes as a function of gap size, we firstly trace the positions of the EELS peaks for the BQM and BDM in Figure 6a and the ADM in Figure 6b by the thick-dashed gray curves. Then the experimentally measured resonant energies of these modes are extracted and plotted versus the gap size in **Figure 6c** (see the symbols), and compared with the numerical results (see the lines). On the one hand, the resonant energy of the BDM predicted by different numerical models has different variation trend as the gap size changes. As gap size decreasing, the nonlocal results (red dashed line) show slower red-shift evolution trend than the classical results (red solid line). As the gap size further reduces to smaller than 0.3 nm, the QCM results (purple dash-dotted line) predict that the BDM is quenched and the high order CTM appears with the blue-shift trend. The numerical results clearly illustrate the critical role of spatial nonlocality and quantum tunneling effect in altering the palsmon properties of the BDM. For the higher order bonding mode, i.e. the BQM, the experimental measured resonance energy (green symbols) shows insensitivity to the gap size, which agrees with the numerical results (green line). This indicates that the BQM is not affected by the nonlocal and quantum tunneling effect. However, without clear observation of the BDM and CTM resonances on the EELS spectra of dimers with gap sizes below 3 nm (Figure 6a), the quantum effect of the dimer under edge excitation is difficult to be verified by present experimental results. On the other hand, when the dimer is excited by the center electron beam the measured resonant energies of the ADM (blue symbols) agree well with the

numerical results (blue line), implying the robustness of the ADM to the gap size and environment variation. We should note that the gold nanospheres in the fabricated dimers are not perfectly identical or spherical (see **Figure 6**). Therefore, the size difference between the coupled nanospheres could break the mirror symmetry of the whole dimer. Such symmetry breaking makes it possible to weakly excite the ADM (BDM) by the center (edge) electron beam.[53] Another possible geometry factor that may have influence on the EELS spectra of the dimers is the facets near the gap regions. It has been demonstrated that a new set of

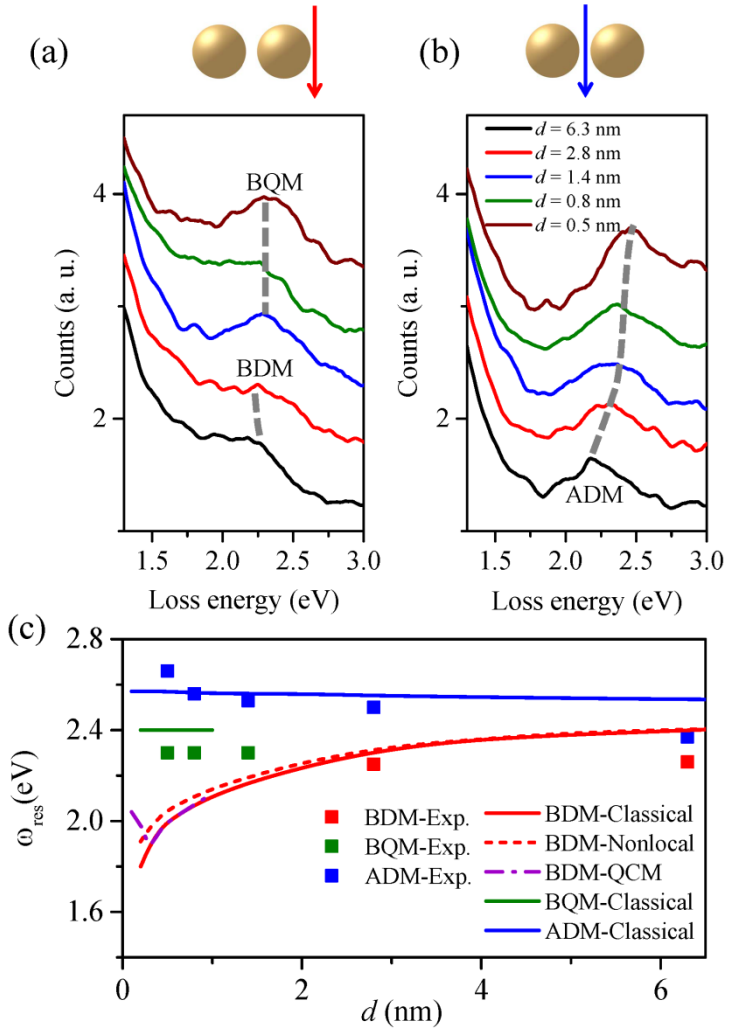

Figure 6. Measured EELS spectra of five gold nanosphere dimers with varied gap size under a) the edge excitation and b) the center excitation. The gray-dashed curves trace the EELS energies of the BDM, BQM and ADM resonances. c) The experimental (symbols) and calculated (lines) energies of BDM, BQM and ADM versus the gap size. The resonant energies of the BDM obtained by classical (red solid line), nonlocal (red dashed line) and QCM (purple dash-dotted line) has different variation trends as the gap size changes. For the resonant energies of the BQM and ADM, different calculation models predict the same variation trend.

resonant modes, namely transverse cavity plasmons (TCPs), may be induced in small gap regions with flat facets. When these TCPs overlap with the BDMs, the mode coupling can happen, resulting in Fano-like anticrossing features in the spectra.[78] As a matter of fact, the impact of the quantum tunneling on the spectra of dimers is intimately related to the morphology of nanogaps. Typically, the lowest order CTM blue shifts as the gap morphology changes from curved faces to planer faces.[79] But for small facets in other regions (not in the gap) as observed in the HAADF images of the dimers in Figure 5, they have small influence on the plasmon properties of the dimer.

3. Conclusions

In summary, we have investigated the spatial nonlocality and quantum tunneling effects in the plasmonic bright (BDM) and dark modes (ADM) of gold nanosphere homodimers by a comparative numerical and experimental EELS study. The numerical EELS spectra of the BDM obtained using classical and quantum models evolve distinctively as the gap size between the gold nanospheres goes to zero, revealing the remarkable influences of the quantum effects on the plasmonic property of the bright mode. In sharp contrast, the EELS responses of the ADM obtained with different models are quite comparable and robust versus the varying gap size. This indicates that the optically dark mode is unlikely affected by the quantum mechanical effects, especially the electron tunneling cannot even occur in the ADM. Experimentally, the BMD resonances are unrecognizable for dimers with small gaps under the edge excitation while the features of the ADM are obvious for all the dimers under center excitation. These experimental observations qualitatively agree with the numerical predictions, further confirming the different impacts of the quantum tunneling effects on the bright and dark modes in the dimers. Although the present study is on the simplest plasmonic nanoparticle assemblies, i.e. dimers, the significant differences of the quantum effects on bright and dark plasmon modes are expected to be universal in any coupled plasmonic

nanostructures with small gaps. We believe that our results give more insights into the quantum mechanical effects in plasmonics and may be helpful in designing sophisticated optical nanocavities with atomic-scale gaps.

Experimental Section

Experimental EELS Characterization: STEM imaging and EELS mapping were carried out on a Cs-corrected JEOL ARM200F STEM equipped with a Gatan Enfinium ER spectrometer, operating at 200 kV and with a cold field emission gun (CFEG) without a monochromator. The EELS energy resolution is ~0.3 eV as measured from the FWHM of the zero-loss peak. A beam convergence semi-angle of 26 mrad and an EELS collection semi-angle of 18 mrad were used. The spectrometer dispersion was set to 0.01 eV per channel with an acquisition time of 50 ms per pixel for the EELS mapping. Annular-dark-field (ADF) images were recorded simultaneously with the EEL spectra using an inner semi-angle of around 60 mrad.

EELS calculation in a local classical electromagnetic simulation: For a fast moving electron along a straight-line trajectory $\mathbf{r}_e(t)$, its energy loss ΔE reads:[59]

$$\Delta E = e\int dt\,\mathbf{v}\cdot\mathbf{E}^{\mathrm{ind}}[\mathbf{r}_e(t),t] = \int_0^\infty \hbar\omega d\omega\,\Gamma_{\mathrm{EELS}}(\omega), \tag{1}$$

where e is the charge of the electron, $\mathbf{v}$ is the relativistic speed of the electron, $\mathbf{E}^{\mathrm{ind}}$ is the external induced electric field, $\hbar$ is the reduced Planck constant, ω is the angular frequency, and $\Gamma_{\mathrm{EELS}}(\omega)$ is the electron energy loss probability. Assuming the electron moves in z-direction, with some algebraic operations Γ_{EELS} can then be calculated by a line integration as:[59, 66]

$$\Gamma_{\mathrm{EELS}}(\omega) = \frac{e}{\pi\hbar\omega}\int dz\,\mathrm{Re}[E_z^{\mathrm{ind}}(\omega,z)\exp(-i\omega z/\mathbf{v})]. \tag{2}$$

In Equation (2), E_z^{ind} is the *z*-component of the induced electric field which is calculated by a two-step electromagnetic simulation. The first step is to compute the radiation field of the electron beam in vacuum (without any particle) from a z-direction line current with the current density $\mathbf{j}(\mathrm{z},\omega)$ of:

$$\mathbf{j}(z,\omega) = -e\hat{\mathbf{z}} \cdot \exp(i\omega z/\mathbf{v}). \tag{3}$$

Then the calculated radiation field of the electron beam in the first step is used as a background field $\mathbf{E}_{\mathrm{b}}$ in the second step to obtain the scattered field by the particle, i.e. the induced field $\mathbf{E}^{\mathrm{ind}}$. In both steps, a perfect matched layer (PML) is used as the boundary condition. In the classical local calculations, the permittivity of gold $\varepsilon_{\mathrm{m}}(\omega)$ is taken from a fitting of the empirical data.[80]

Nonlocal EELS calculation by a Hydrodynamic Model: In the nonlocal EELS calculations, the total electromagnetic fields $\mathbf{E}(\mathrm{r},\omega)$ and current density $\mathbf{J}(\omega,\mathrm{z})$ in the metal regions are computed by solving the coupled Equations (4) and (5) of the hydrodynamic model with an additional boundary conditions (ABC) $\mathbf{n}\cdot\mathbf{J}(\mathbf{r},\omega)=0$ at the boundaries of the metal, where $\mathbf{n}$ is the normal vector of the metal surface.[47,66]

$$\nabla\times\nabla\times\mathbf{E}(\mathbf{r},\omega) = k_0^2\varepsilon_{\mathrm{core}}(\omega)\mathbf{E}(\mathbf{r},\omega) + i\omega\mu_0\mathbf{J}(\mathbf{r},\omega), \tag{4}$$

$$\beta^2\nabla[\nabla\cdot\mathbf{J}(\mathbf{r},\omega)] + \omega(\omega+i\gamma_0)\mathbf{J}(\mathbf{r},\omega) = i\varepsilon_0\omega\omega_{\mathrm{p}}^2\mathbf{E}(\mathbf{r},\omega), \tag{5}$$

Where k_0 is the wave vector in the vacuum, ε_0 (μ_0) is the permittivity (permeability) of the vacuum, $\varepsilon_{\mathrm{core}}(\omega)$ is the local permittivity of gold responsible for the bound ions and electrons, β is the nonlocal parameter, γ_0 and ω_p are the collision and plasmon frequency of the Drude-model for gold. In the high-frequency limit ($\omega \gg \gamma_0$), the nonlocal parameter β is related to the Fermi velocity $v_{\mathrm{F}} = 1.39\times10^6$ m/s via $\beta^2 = 3v_F^2/5$. In our simulation, $\varepsilon_{\mathrm{core}}(\omega)$ of

gold is obtained by subtracting the Drude part from the empirical data, i.e. $\varepsilon_{\text{core}}(\omega)=\varepsilon_{\text{m}}(\omega)+\omega_{\text{p}}^2/(\omega^2+i\gamma_0\omega)$, where $\hbar\gamma_0=0.71$ eV and $\hbar\omega_{\text{p}}=9.02$ eV.[49]

Implement of the Quantum-Corrected Model in the EELS calculation: The quantum corrected model (QCM) is a classical electromagnetic simulation method to study the quantum tunneling effect in plasmonic nanostructures with atomic scale gaps. The validity of the QCM has been verified by comparing their calculated optical properties with fully quantum-mechanical results in various kinds of coupled plasmonic nanoparticles.[35, 36, 40] The implementation of the QCM needs to introduce a fictional medium in the gap region as sketched in Figure 7. Such fictional medium has an inhomogeneous and local-separation l dependent permittivity $\varepsilon_{\text{g}}(\omega,l)$ given by Equation (6),[40, 71]

$$\varepsilon_{\text{g}}(\omega,l)=\varepsilon_0-\frac{\omega_{\text{p}}^2}{\omega^2+i\gamma_{\text{g}}(\omega,\text{l})\omega}+\left[\varepsilon_{\text{core}}(\omega)-\varepsilon_0\right]\exp(\frac{-l}{l_d}), \tag{6}$$

where $\gamma_{\text{g}}(\omega,l)=\gamma_0\exp^{l/l_c}$ and the parameter l_c is determined by the tunneling conductivity obtained from a static scanning tunneling microscopy approach. The remaining parameter in Equation (6) is the decay length l_d of the *d*-electron contribution. For gold, we choose $l_c=0.04$ nm and $l_d=0.079$ nm from Ref [71]. From equation (6) we can find when $l\to 0$, $\varepsilon_g(\omega,l)\to\varepsilon_m(\omega)$, therefore the fictional medium would be gold-like. In this situation, the electron beam at the center excitation actually penetrates a lossy material, resulting in an extra bulk loss.

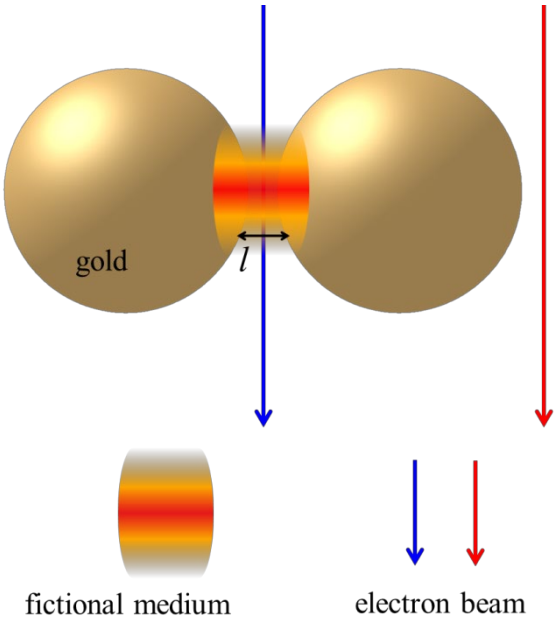

Figure 7. Schematic of implementation of the QCM in gold dimers excited by electron beams.

Acknowledgements
We acknowledge the financial support by the National Natural Science Foundation of China (Grant No. 11474240), the Hong Kong Research Grants Council (Grant Nos. 25301617, C6021-14E, and SBI17SC16), the Hong Kong Polytechnic University (Grant Nos. 1-ZE6G and 4-BCCB), and the technical support of the high-resolution electron microscopy facility at MCPF of the Hong Kong University of Science and Technology. Part of this work was funded by the Deutsche Forschungsgemeinschaft (DFG grant PA 794/28-1).

Received: ((will be filled in by the editorial staff))
Revised: ((will be filled in by the editorial staff))
Published online: ((will be filled in by the editorial staff))

References

[1] K. A. Willets, R. P. Van Duyne, Localized surface plasmon resonance spectroscopy and sensing. *Annu. Rev. Phys. Chem.* **2007,** *58*, 267.
[2] W. L. Barnes, A. Dereux, T. W. Ebbesen, Surface plasmon subwavelength optics. *Nature* **2009,** *424*, 824.
[3] E. Hutter, J. H. Fendler, Exploitation of localized surface plasmon resonance. *Adv. Mater.* **2004**, *16,* 1685.
[4] K. L. Kelly, E. Coronado, L. L. Zhao, G. C. Schatz, The optical properties of metal nanoparticles: the influence of size, shape, and dielectric environment. *J. Phys. Chem. B* **2003**, *107,* 668.
[5] P. L. Stiles, J. A. Dieringer, N. C. Shah, R. P. Van Duyne, Surface-enhanced Raman spectroscopy. *Annu. Rev. Phys. Chem.* **2008,** *1*, 601.
[6] K. Chen, X. Zhang, Y. Zhang, D. Y. Lei, H. Li, T. Williams, D. R. Macfarlane, Highly ordered Ag/Cu hybrid nanostructure arrays for ultrasensitive surface-enhanced Raman spectroscopy. *Adv. Mater. Interfaces* **2016,** *3*, 1600115.

[7] C. E. Talley, J. B. Jackson, C. Oubre, N. K. Grady, C. W. Hollars, S. M. Lane, T. R. Huser, P. Nordlander, N. J. Halas, Surface-enhanced Raman scattering from individual Au nanoparticles and nanoparticle dimer substrates. *Nano Lett.* **2005,** *5*, 1569.
[8] A. J. Haes, R. P. Van Duyne, A unified view of propagating and localized surface plasmon resonance biosensors. *Anal. Bioanal. Chem.* **2004,** *379*, 920.
[9] J. I. Chen, Y. Chen, D. S. Ginger, Plasmonic nanoparticle dimers for optical sensing of DNA in complex media. *J. Am. Chem. Soc.* **2010,** *132*, 9600.
[10] Z. Yong, D. Y. Lei, C. H. Lam, Y. Wang, Ultrahigh refractive index sensing performance of plasmonic quadrupole resonances in gold nanoparticles. *Nanoscale Res. Lett.* **2014,** *9*, 187.
[11] R. Naraoka, H. Okawa, K. Hashimoto, K. Kajikawa, Surface plasmon resonance enhanced second-harmonic generation in Kretschmann configuration. *Opt. Commun.* **2005,** *248*, 249.
[12] B. L. Wang, M. L. Ren, J. F. Li, Z. Y. Li, Plasmonic coupling effect between two gold nanospheres for efficient second-harmonic generation. *J. Appl. Phys.* **2012,** *112*, 083102.
[13] S. Zhang, G. C. Li, Y. Chen, X. Zhu, S. D. Liu, D. Y. Lei, H. Duan, Pronounced Fano resonance in single gold split nanodisks with 15 nm split gaps for intensive second harmonic generation. *ACS Nano* **2016,** *10*, 11105.
[14] N. Engheta, Circuits with light at nanoscales: Optical nanocircuits inspired by metamaterials. *Science* **2007,** *317*, 1698.
[15] V. J. Sorger, R. F. Oulton, R.-M. Ma, X. Zhang, Toward integrated plasmonic circuits. *MRS Bulletin* **2012,** *37*, 728.
[16] V. E. Ferry, L. A. Sweatlock, D. Pacifici, H. A. Atwater, Plasmonic nanostructure design for efficient light coupling into solar cells. *Nano Lett.* **2008,** *8*, 4391.
[17] N. Fu, Z. Y. Bao, Y. L. Zhang, G. Zhang, S. Ke, P. Lin, J. Dai, H. Huang, D. Y. Lei, Panchromatic thin perovskite solar cells with broadband plasmonic absorption enhancement and efficient light scattering management by Au@Ag core-shell nanocuboids. *Nano Energy* **2017,** *41*, 654.
[18] A. Aubry, D. Y. Lei, A. I. Fernández-Domínguez, Y. Sonnefraud, S. A. Maier, J. B. Pendry, Plasmonic light-harvesting devices over the whole visible spectrum. *Nano Lett.* **2010,** *10* (7), 2574.
[19] J. T. Li, S. K. Cushing, F. K. Meng, T. R. Senty, A. D. Bristow, N. Q. Wu, Plasmon-induced resonance energy transfer for solar energy conversion. *Nat. Photon.* **2015,** *9*, 601.
[20] H. Wang, P. Liu, Y. Ke, Y. Su, L. Zhang, N. Xu, S. Ding, and H. Chen, Dimers exhibiting unidirectional visible light scattering and strong electromagnetic field enhancement. *ACS Nano* **2015**, *9*, 436.
[21] J. Wen, H. Wang, W. Wang, Z. Deng, C. Zhuang, Y. Zhang, F. Liu, J. She, J. Chen, H. Chen, S. Deng, N. Xu, Room-temperature strong light−matter interaction with active control in single plasmonic nanorod coupled with two-dimensional atomic crystals. *Nano Lett*. **2017**, *17*, 4689.
[22] P. Nordlander, C. Oubre, E. Prodan, K. Li, M. I. Stockman, Plasmon hybridization in nanoparticle dimers. *Nano Lett.* **2004,** *4*, 899.
[23] E. Prodan, C. Radloff, N. J. Halas, P. Nordlander, A hybridization model for the plasmon response of complex nanostructures. *Science* **2003,** *302*, 419.
[24] A. Aubry, D. Y. Lei, S. A. Maier, J. B. Pendry, Plasmonic hybridization between nanowires and a metallic surface: a transformation optics approach. *ACS Nano* **2011,** *5*, 3293.
[25] Q. Liang, Y. Wen, X. Mu, T. Reindl, W. Yu, N. Talebi, P. A. van Aken, Investigating hybridization schemes of coupled split-ring resonators by electron impacts. *Opt. Express* **2015,** *23*, 20721.

[26] A. M. Funston, C. Novo, T. J. Davis, P. Mulvaney, Plasmon coupling of gold nanorods at short distances and in different geometries. *Nano Lett.* **2009,** *9*, 1651.
[27] P. Nordlander, E. Prodan, Plasmon hybridization in nanoparticles near metallic surfaces. *Nano Lett.* **2004,** *4*, 2209.
[28] S. Sheikholeslami, Y. W. Jun, P. K. Jain, A. P. Alivisatos, Coupling of optical resonances in a compositionally asymmetric plasmonic nanoparticle dimer. *Nano Lett.* **2010,** *10*, 2655.
[29] O. L. Muskens, V. Giannini, J. A. Sánchez-Gil, J. Gomez Rivas, Optical scattering resonances of single and coupled dimer plasmonic nanoantennas. *Opt. Express* **2007,** *15*, 17736.
[30] B. Khlebtsov, A. Melnikov, V. Zharov, N. Khlebtsov, Absorption and scattering of light by a dimer of metal nanospheres: comparison of dipole and multipole approaches. *Nanotechnology* **2006,** *17*, 1437.
[31] A. E. Schlather, N. Large, A. S. Urban, P. Nordlander, N. J. Halas, Near-field mediated plexcitonic coupling and giant Rabi splitting in individual metallic dimers. *Nano Lett.* **2013,** *13*, 3281.
[32] S. S. Aćimović, M. P. Kreuzer, M. U. Gonzalez, R. Quidant, Plasmon near-field coupling in metal dimers as a step toward single-molecule sensing. *ACS Nano* **2009,** *3*, 1231.
[33] H. Aouani, M. Rahmani, M. Navarro-Cia, S. A. Maier, Third-harmonic-upconversion enhancement from a single semiconductor nanoparticle coupled to a plasmonic antenna. *Nat. Nanotech.* **2014,** *9*, 290.
[34] V. V. Thacker, L. O. Herrmann, D. O. Sigle, T. Zhang, T. Liedl, J. J. Baumberg, U. F. Keyser, DNA origami based assembly of gold nanoparticle dimers for surface-enhanced Raman scattering. *Nat. Commun.* **2014,** *5*, 3448.
[35] W. Zhu, R. Esteban, A. G. Borisov, J. J. Baumberg, P. Nordlander, H. J. Lezec, J. Aizpurua, K. B. Crozier, Quantum mechanical effects in plasmonic structures with subnanometre gaps. *Nat. Commun.* **2016,** *7*, 11495.
[36] W. Zhu, K. B. Crozier, Quantum mechanical limit to plasmonic enhancement as observed by surface-enhanced Raman scattering. *Nat. Commun.* **2014,** *5*, 5228.
[37] L. Yang, H. Wang, Y. Fang, Z. Li, Polarization state of light scattered from quantum plasmonic dimer antennas. *ACS Nano* **2016,** *10*, 1580.
[38] H. Cha, D. Lee, J. H. Yoon, S. Yoon, Plasmon coupling between silver nanoparticles: Transition from the classical to the quantum regime. *J. Colloid Interf. Sci.* **2016,** *464*, 18.
[39] H. Cha, J. H. Yoon, S. Yoon, Probing quantum plasmon coupling using gold nanoparticle dimers with tunable interparticle distances down to the subnanometer range. *ACS Nano* **2014,** *8*, 8554.
[40] R. Esteban, A. G. Borisov, P. Nordlander, J. Aizpurua, Bridging quantum and classical plasmonics with a quantum-corrected model. *Nat. Commun.* **2012,** *3*, 825.
[41] S. Kadkhodazadeh, J. B. Wagner, H. Kneipp, K. Kneipp, Coexistence of classical and quantum plasmonics in large plasmonic structures with subnanometer gaps. *Appl. Phys Lett.* **2013,** *103* (8), 083103.
[42] G. Hajisalem, M. S. Nezami, R. Gordon, Probing the quantum tunneling limit of plasmonic enhancement by third harmonic generation. *Nano Lett.* **2014,** *14*, 6651.
[43] D. C. Marinica, A. K. Kazansky, P. Nordlander, J. Aizpurua, A. G. Borisov, Quantum plasmonics: nonlinear effects in the field enhancement of a plasmonic nanoparticle dimer. *Nano Lett.* **2012,** *12*, 1333.
[44] K. J. Savage, M. M. Hawkeye, R. Esteban, A. G. Borisov, J. Aizpurua, J. J. Baumberg, Revealing the quantum regime in tunnelling plasmonics. *Nature* **2012,** *491*, 574.
[45] J. A. Scholl, A. García-Etxarri, A. L. Koh, J. A. Dionne, Observation of quantum tunneling between two plasmonic nanoparticles. *Nano Lett.* **2013,** *13*, 564.

[46] S. F. Tan, L. Wu, J. K. Yang, P. Bai, M. Bosman, C. A. Nijhuis, Quantum plasmon resonances controlled by molecular tunnel junctions. *Science* **2014,** *343*, 1496.
[47] C. David, F. J. García de Abajo, Spatial nonlocality in the optical response of metal nanoparticles. *J. Phys. Chem. C* **2011,** *115*, 19470.
[48] F. J. G. de Abajo, Nonlocal effects in the plasmons of strongly interacting nanoparticles, dimers, and waveguides. *J. Phys. Chem. C* **2008,** *112*, 17983.
[49] S. Raza, S. I. Bozhevolnyi, M. Wubs, N. Asger Mortensen, Nonlocal optical response in metallic nanostructures. *J. Phys. Condens. Matter* **2015,** *27*, 183204.
[50] P. K. Jain, W. Y. Huang, M. A. El-Sayed, On the universal scaling behavior of the distance decay of plasmon coupling in metal nanoparticle pairs: A plasmon ruler equation. *Nano Lett.* **2007,** *7*, 2080.
[51] S. Kadkhodazadeh, J. R. de Lasson, M. Beleggia, H. Kneipp, J. B. Wagner, K. Kneipp, Scaling of the surface plasmon resonance in gold and silver dimers probed by EELS. *J. Phys. Chem. C* **2014,** *118*, 5478.
[52] C. Ciracì, R. T. Hill, J. J. Mock, Y. Urzhumov, A. I. Fernández-Domínguez, S. A. Maier, J. B. Pendry, A. Chilkoti, D. R. Smith, Probing the ultimate limits of plasmonic enhancement. *Science* **2012,** *337*, 1072.
[53] G. C. Li, Y. L. Zhang, J. Jiang, Y. Luo, D. Y. Lei, Metal-substrate-mediated plasmon hybridization in a nanoparticle dimer for photoluminescence line-width shrinking and intensity enhancement. *ACS Nano* **2017,** *11*, 3067.
[54] G. C. Li, Y. L. Zhang, D. Y. Lei, Hybrid plasmonic gap modes in metal film-coupled dimers and their physical origins revealed by polarization resolved dark field spectroscopy. *Nanoscale* **2016,** *8*, 7119.
[55] A. L. Koh, K. Bao, I. Khan, W. E. Smith, G. Kothleitner, P. Nordlander, S. A. Maier, D. W. McComb, Electron energy-loss spectroscopy (EELS) of surface plasmons in single silver nanoparticles and dimers: influence of beam damage and mapping of dark modes. *ACS Nano* **2009,** *3*, 3015.
[56] S. C. Quillin, C. Cherqui, N. P. Montoni, G. Li, J. P. Camden, D. J. Masiello, Imaging plasmon hybridization in metal nanoparticle aggregates with electron energy-loss spectroscopy. *J. Phy. Chem. C* **2016,** *120*, 20852.
[57] A. Hörl, A. Trügler, U. Hohenester, Full Three-dimensional reconstruction of the dyadic Green tensor from electron energy loss spectroscopy of plasmonic nanoparticles. *ACS Photonics* **2015,** *2*, 1429.
[58] A. Hörl, A. Trügler, U. Hohenester, Tomography of particle plasmon fields from electron energy loss spectroscopy. *Phys. Rev. Lett.* **2013,** *111*, 076801.
[59] C. Colliex, M. Kociak, O. Stéphan, Electron energy loss spectroscopy imaging of surface plasmons at the nanometer scale. *Ultramicroscopy* **2016,** *162*, A1.
[60] N. W. Bigelow, A. Vaschillo, V. Iberi, J. P. Camden, D. J. Masiello, Characterization of the electron- and photon-driven plasmonic excitations of metal nanorods. *ACS Nano* **2012,** *6*, 7497.
[61] F. J. García de Abajo, Optical excitations in electron microscopy. *Rev. Mod. Phys.* **2010,** *82*, 209.
[62] A. L. Koh, A. I. Fernández-Domínguez, D. W. McComb, S. A. Maier, J. K. Yang, High-resolution mapping of electron-beam-excited plasmon modes in lithographically defined gold nanostructures. *Nano Lett.* **2011,** *11*, 1323.
[63] M. W. Chu, V. Myroshnychenko, C. H. Chen, J. P. Deng, C. Y. Mou, F. J. G. de Abajo, Probing bright and dark surface-plasmon modes in individual and coupled noble metal nanoparticles using an electron beam. *Nano Lett.* **2009,** *9*, 399.
[64] S. J. Barrow, S. M. Collins, D. Rossouw, A. M. Funston, G. A. Botton, P. A. Midgley, P. Mulvaney, Electron energy loss spectroscopy investigation into symmetry in gold trimer and tetramer plasmonic nanoparticle structures. *ACS Nano* **2016,** *10*, 8552.

[65] J. A. Scholl, A. L. Koh, J. A. Dionne, Quantum plasmon resonances of individual metallic nanoparticles. *Nature* **2012,** *483*, 421.
[66] A. Wiener, H. Duan, M. Bosman, A. P. Horsfield, J. B. Pendry, J. K. Yang, S. A. Maier, A. I. Fernández-Domínguez, Electron-energy loss study of nonlocal effects in connected plasmonic nanoprisms. *ACS Nano* **2013,** *7*, 6287.
[67] J. A. Scholl, A. Garcia-Etxarri, G. Aguirregabiria, R. Esteban, T. C. Narayan, A. L. Koh, J. Aizpurua, J. A. Dionne, Evolution of plasmonic metamolecule modes in the quantum tunneling regime. *ACS Nano* **2016,** *10*, 1346.
[68] S. Raza, G. Toscano, A.-P. Jauho, M. Wubs, N. A. Mortensen, Unusual resonances in nanoplasmonic structures due to nonlocal response. *Phys. Rev. B* **2011,** *84*, 121412(R).
[69] T. Christensen, W. Yan, S. Raza, A. P. Jauho, N. A. Mortensen, M. Wubs, Nonlocal response of metallic nanospheres probed by light, electrons, and atoms. *ACS Nano* **2014,** *8*, 1745.
[70] N. A. Mortensen, S. Raza, M. Wubs, T. Søndergaard, S. I. Bozhevolnyi, A generalized non-local optical response theory for plasmonic nanostructures. *Nat. Commun.* **2014,** *5*, 3809.
[71] R. Esteban, A. Zugarramurdi, P. Zhang, P. Nordlander, F. J. Garcíavidal, A. G. Borisov, J. Aizpurua, A classical treatment of optical tunneling in plasmonic gaps: extending the quantum corrected model to practical situations. *Faraday Discuss.* **2015,** *178*, 151.
[72] G. Toscano, Semiclassical theory of nonlocal plasmonic excitation in metallic nanostructures (PhD Thesis, Department of Photonics Engineering, Technical Univ. Denmark, **2013**.)
[73] Y. Luo, A. I. Fernández-Domínguez, A. Wiener, S. A. Maier, J. B. Pendry, Surface plasmons and nonlocality: a simple model. *Phys. Rev. Lett.* **2013,** *111*, 093901.
[74] X. Yu, D. Y. Lei, F. Amin, R. Hartmann, G. P. Acuna, A. Guerrero-Martínez, S. A. Maier, P. Tinnefeld, S. Carregal-Romero, W. J. Parak, Distance control in-between plasmonic nanoparticles via biological and polymeric spacers. *Nano Today* **2013,** *8*, 480.
[75] A. S. Eggeman, R. Krakow, P. A. Midgley, Scanning precession electron tomography for three-dimensional nanoscale orientation imaging and crystallographic analysis. *Nat. Commun.* **2015**, *6*, 7267.
[76] P. Ercius, O. Alaidi, M. J. Rames, G. Ren, Electron tomography: A three-dimensional analytic tool for hard and soft materials research, *Adv. Mater.* **2015**, *27*, 5638.
[77] C. C. Chen, C. Zhu, E. R. White, C. Y. Chiu, M. C. Scott, B. C. Regan, L. D. Maks, Y. Huang, J. Miao, Three-dimensional imaging of dislocations in a nanoparticle at atomic resolution, *Nature* **2013**, *496*, 74.
[78] R. Esteban, G. Aguirregabiria, A. G. Borisov, Y. M. Wang, P. Nordlander, G. W. Bryant, J. Aizpurua, The morphology of narrow gaps modifies the plasmonic response. *Acs Photonics* **2015,** *2*, 295.
[79] D. Knebl, A. Hörl, A. Trügler, J. Kern, J. R. Krenn, P. Puschnig, U. Hohenester, Gap plasmonics of silver nanocube dimers. *Phys. Rev. B* **2016,** *93*, 081405(R).
[80] P. B. Johnson, Optical constants of the noble metals. *Phys.Rev. B* **1972,** *6*, 4370.